Temperature dependent device characteristics of graphene/h-BN/Si heterojunction

Temperature Dependent Device Characteristics of Graphene/h-BN/Si Heterojunction

Chen Wang, Sanjay K. Behura*, and Vikas Berry*

Department of Chemical Engineering, University of Illinois at Chicago, 810 S. Clinton Street, Illinois 60607, United States

Corresponding authors. sbehura1@uic.edu and vikasb@uic.edu

Graphene-on-semiconductor heterojunction solar cell is an emerging class of photovoltaics with potential for efficient and reliable energy conversion systems. The interfaces between graphene and lightly-doped semiconductor play a key role in charge-carrier separation and recombination dynamics. Owing to the low Schottky barrier height-induced interfacial charge carrier recombination, the graphene-on-silicon (Si) heterojunction solar cells suffer from instability in power conversion efficiency over time. Therefore, it is critical to engineer the interface to enhance the barrier height by interfacing a chemically-stable, insulating, and atomically-thin layer. Further, the temperature dependent photovoltaic characteristics of such stacked architectures are unknown, and temperature dependent behavior is critical to understand the MIS junction behavior and photovoltaic phenomenon. Here, we have introduced hexagonal boron nitride (h-BN) as a tunneling interlayer in graphene-on-Si heterojunction solar cells, which enables the passivation of the chemical dangling bonds on the Si surface. The effect of temperature on the performance of graphene/h-BN/Si PV cell is examined. Thin films of h-BN are directly synthesized on lightly-doped Si surface *via* a bottom-up chemical-surface-adsorption strategy followed by the transfer of a graphene monolayer. The 2D layer-on-2D layer-on-3D bulk semiconductor nanoarchitecture of graphene/h-BN/Si forms a metal-insulator-semiconductor (MIS)-type junction, where the h-BN acts as an electron-blocking layer to avoid interfacial charge carrier recombination. A 4-fold increase in open-circuit voltage (V_{OC}) is found for graphene/h-BN/Si heterojunction cell (0.52 V) in contrast to the graphene/Si cell (0.13 V), which is due to the increase in the Schottky barrier height and hence built-in electric potential. Interestingly, the V_{OC} linearly decreases by only ~4% with every 10 K increase in temperature. This work will lead to an evolution of new 2D/2D/3D nanoarchitectures for mechanically-robust, high performance, and durable optoelectronic functionalities.

INTRODUCTION

Owing to the high optical transparency and ultra-high charge carrier mobility, sp^2-hybridized graphene[1–3], which can function both as a transparent electrode and an active layer, is a potential candidate two-dimensional (2D) material for photonics, optoelectronics, and photovoltaics. A rectifying Schottky junction can be constructed by interfacing graphene with lightly doped Si , which can be employed as a photovoltaic cell[4] under the irradiation of light. The graphene-on-semiconductor heterostructure, which benefits from cost-effective fabrication process, has shown promising power conversion efficiency of over 10% at AM 1.5G irradiation with functionalized or doped graphene[5–11] and with an anti-reflection layer[12–15]. However, the graphene/Si-based 2D layer-on-3D bulk semiconductor solar cell suffers from serious instability in the photovoltaic performance.[16] This stems from the existence of an astronomically high dark-current in the graphene/Si Schottky barrier junctions, which is caused by the thermionic-emission based dark current.[17] What's more, mid-gap surface states can be formed by dangling bonds on the Si surface, which will provide additional pathway for the charge carrier recombination.[18]

To reduce the thermionic-emission based dark current and charge-carrier recombination, a non-reactive and stable passivation layer is required to separate metal and semiconductor by forming a metal/insulator/semiconductor (MIS) architecture.[19] Previously, thin film insulators like transferred h-BN[20], silicon dioxide (SiO_2)[21] ,Al_2O_3[22] and fluorographene (FG)[23] have been reported as an electron blocking layer in MIS structure for photovoltaic application. Unlike SiO_2 and fluorographene,[21] the h-BN layer does not have trap-charges and surface states.[24,25] Hexagonal boron nitride (h-BN) is a sp^2-hybridized 2D insulator with wide energy bandgap of 5.97 eV and ultra-smooth surface with no surface-dangling-bonds[26–28]. Further, the h-BN is isostructural and isoelectronic to graphene with lattice mismatching of only 1.7%, thus enabling compatible graphene/h-BN heterostructure.[29] Similar MIS structure has been built by transferring the h-BN layer[30] on Si surface, which can introduce heteroatom contaminations during chemical-transfer process.[31] Therefore, direct growth of h-BN on Si surfaces is critical to avoid the defects and for scalability. The temperature dependent diode and photovoltaic characteristics of the graphene/h-BN/n-Si heterojunction solar cell can be crucial to understand the charger carrier separation and recombination dynamics at the MIS structure interface. Previously, Kalita et al. investigated temperature dependent study on metal-semiconductor (MS)-type graphene-GaN heterojunction and MIS-type graphene/h-BN/GaN in the range of 298 to 373 K.[32,33] Graphene-GaN heterojunction showed photovoltaic effect and its V_{oc} decreased nonlinearly with the temperature. Graphene/h-BN/GaN heterojunction showed increased Schottky barrier height. Temperature dependent study of Si based MIS solar cell has been explored in many previous studies.[34] However, no temperature dependent photovoltaic characteristic of graphene based MIS structure has been reported. It is therefore critical to investigate the temperature dependent photovoltaic characteristics of a graphene/h-BN/n-Si heterojunction device.

In this work, we directly nucleated h-BN layer on n-type silicon (n-Si) surface *via* surface-chemical-interaction mechanism[25,35]. A chemical-vapor deposited single-layer graphene was transferred on top of h-BN to construct a graphene/h-BN/n-Si MIS-type heterostructure. Temperature dependent photovoltaic characteristics is investigated. The open-circuit voltage (V_{OC}) of maximum of 0.52 V is achieved merely by introducing h-BN interlayer, which is of 4-fold increase in comparison to the graphene/n-Si heterojunction cell. An energy-band model is developed to determine the effective Schottky barrier height (ϕ'_{SBH}) of graphene/h-BN/n-Si heterostructure after incorporating the h-BN layer. The temporal-stability of the photovoltaic parameters is investigated to illustrate the robustness and durability of the cell.

EXPERIMENTAL

The fabrication process for a graphene/h-BN/Si solar cell is schematically illustrated in Figure 1 (a) Thin films of h-BN was directly synthesized on 1X1 cm^2 solar grade lightly doped n-Si by low-pressure chemical vapor deposition (LPCVD) as reported in the literature.[25] The process steps are presented in the Materials and Methods section. Monolayer graphene was synthesized on copper foil (99.8%, Alfa-Aesar) using thermal LPCVD and transferred onto h-BN/n-Si chip using the standard PMMA transfer method as reported previously.[36] The copper was removed by immersing PMMA coated graphene/copper into acid solution consisted of 1 part of HNO_3 and 1 part of DI water under ambient temperature for 10 minutes. The PMMA was removed by immersing the graphene-coated sample in the 60 °C-heated-acetone bath for 10 minutes. Both the process of synthesis of graphene on metal catalyst substrates and its chemical transfer are presented in Materials and Methods section. For solar cell fabrications, the Titanium (10 nm)/Gold (50 nm) pattern was made by standard e-beam evaporation and lift-off lithography strategy. The gallium-indium eutectic (99.99% Aldrich) was used as the back-contact metal-electrode for the graphene/h-BN/n-Si cell. Raman spectra were acquired by a confocal Raman microscope (Raman-AFM, WITec alpha 300 RA, laser wavelength of 532 nm and beam size of 721 nm). The light and dark current density/voltage (J-V) characteristic profiles were acquired under AM1.5G illumination (100 mW/cm^2) and dark condition using a Keithley 2612 source-measure-unit. Quantum efficiency measurement (wavelength range: 200-1100 nm) facility was created in-house with the monochromator provided by ORIEL Instrument. The temperature dependent studies were conducted in Janis ST-100 setup.

RESULTS AND DISCUSSION

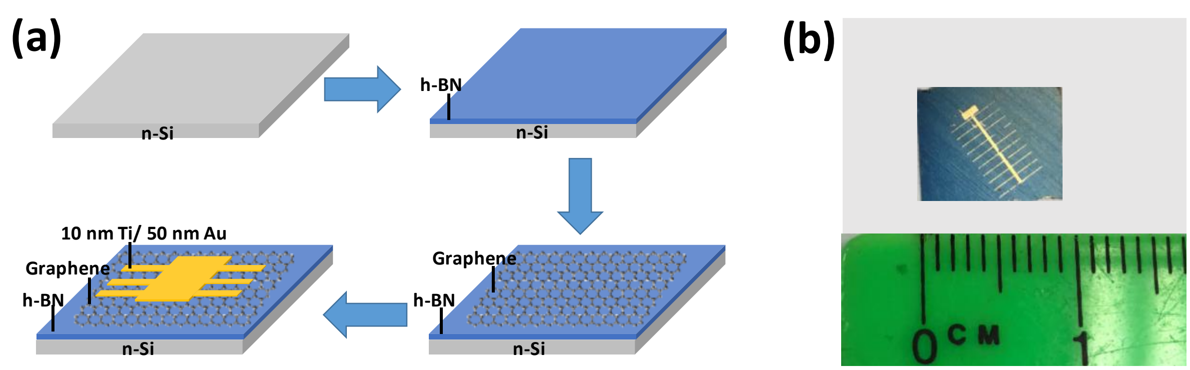

Figure 1. (a) Schematic of the graphene/h-BN/n-Si solar cell development process steps. (b) Optical image of the cell with an effective area of 0.25 cm^2.

Raman vibrational spectroscopy is typically employed to identify chemical and electronic structure by observing vibrational, rotational, and other low-frequency modes in a material system.[18] Raman spectroscopy has been extensively utilized as an inelastic-scattering based finger-print to characterize the 2D nanomaterials.[37–39] Scanning Raman spectra and mapping results are presented in Figure 2 to confirm the nucleation of h-BN on n-Si and formation of graphene/h-BN heterostructure. The presence of a weak peak at 1368.8 cm^{-1} in h-BN/n-Si Raman spectrum (Figure 2 (a)) corresponds to the E_{2g} in-plane vibration of boron and nitrogen atoms in the molecular building unit of h-BN as shown in the inset.[40] There are also no competing Raman peaks such as 1304 cm^{-1} and 1055 cm^{-1} which correspond to the longitudinal optical (LO) phonon and the transversal optical (TO) phonon of c-BN.[39] The color circles (black, green, blue, red and purple) at different area of Figure 2(b) corresponds to the Raman spectrum of the same color in Figure 2(a). The homogeneous color contrast in Figure 2 (b) and presence 1368 cm^{-1} Raman peaks in all the Raman spectra in Figure 1(a) clearly shows a continuous and uniform h-BN film formation on solar grade light p-doped n-Si surfaces.[35] Further, for graphene/h-BN/n-Si hybrid

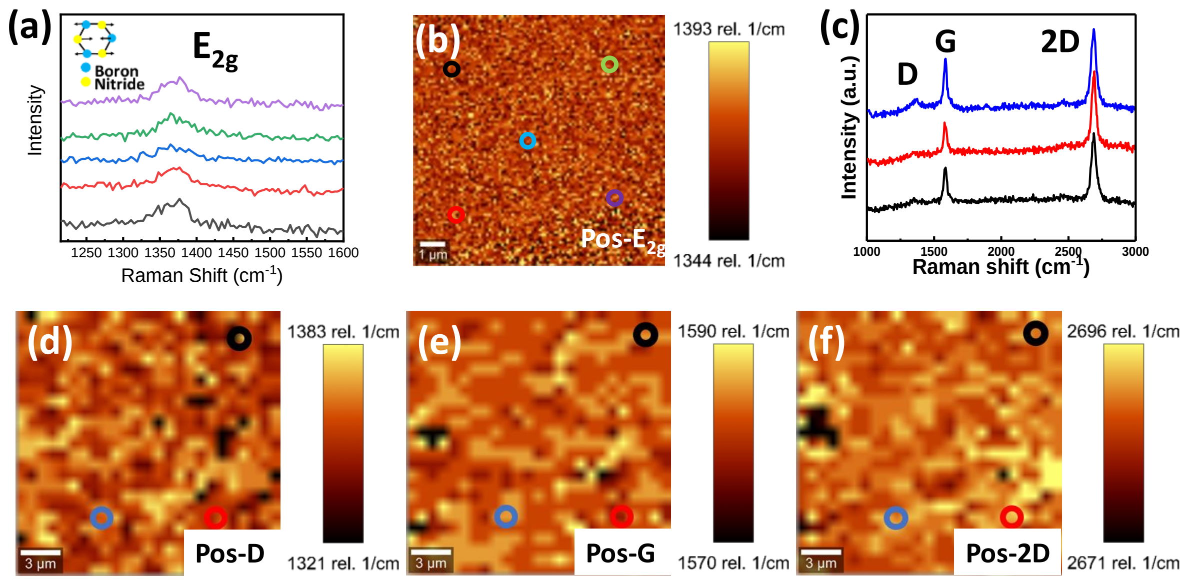

Figure 2. Raman Characterization of h-BN and Graphene/h-BN Heterostructure: (a) Raman spectrum shows the E_{2g} vibrational mode of h-BN produced directly on n-Si surface with the in-plane atomic vibration in the inset, while assorted color lines represent assorted color dots in (b). (b) spatial Raman mapping of h-BN's E_{2g} peak (c) Raman spectra for graphene on h-BN/Si, while assorted color lines represent assorted color dots in (d)-(f). Spatial Raman mapping of graphene's D peak (d), G peak (e), and 2D peak (f).

system, two characteristic Raman modes at 1583 cm^{-1} (G-peak) and 2687 cm^{-1} (2D peak) are found, which demonstrates the continuous interafcing of graphene on h-BN surface. It is noticed that the Raman shift of this graphene's G-peak is less than 1584.5 cm^{-1}, which indicates lightly doped graphene.[41] To further confirm the uniformty of graphene/h-BN heterostrcuture, spatial Raman mapping for graphene's D peak (1344 cm^{-1}), G peak (1583cm^{-1}), and 2D peak (2687cm^{-1}) are presented in Figure 2 (d)–(e). The colored circles (blue, red, and black) at different areas of Figure 2 (d-f) correspond to the Raman spectra of the same color in Figure 2 (c). The homogenous color contrast (Figure 2 (d-f)) clearly shows a continous and uniform transferred graphene on the h-BN/n-Si surface.

Photo-electrical measurements are essential to investigate the perfromance of photovoltaic cells. Figure 3 (a) shows the photovoltaic profile for graphene/h-BN/n-Si solar cell. As expected, the performance of the device with h-BN as an interlayer increased in comparison to the reference graphene/n-Si solar cell. The photovoltaic characteristics such as: open-circuit voltage (V_{oc}), short-circuit current density (J_{sc}) and fill-factor (FF) of the graphene/h-BN/n-Si device are 0.52 V, 0.57 mA/cm^2 and 25%. The measured V_{oc} for graphene/n-Si solar cell is about 0.13 V as shown in the inset. It is intersting to observe that by inserting a thin-film of h-BN layer between graphene and n-Si enhances the V_{oc} by 4-fold. Further, it is critical to understand the recombination dynamics in the graphene/h-BN/n-Si photovoltaic cell. The external quantum efficiency (EQE) is a spectro-electronic tool and it is the ratio of the number of charge carriers collected by the solar cell to the number of incident photons of a given wavelength. As presented

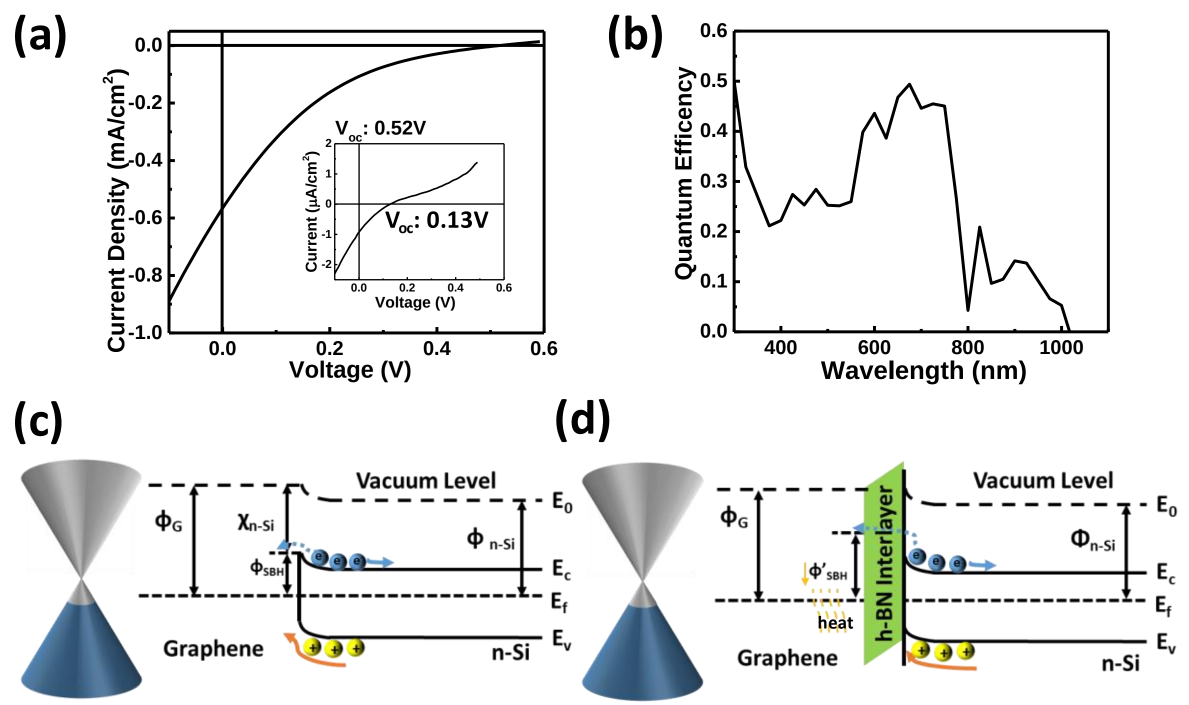

Figure 3. Photovoltaic Measurement on Graphene/h-BN/n-Silicon Solar Cell: (a) Illuminated J-V characteristics of the graphene/h-BN/n-Si solar cell. The inset shows illuminated J-V characteristics of the graphene/Si cell. (b) Quantum efficiency of the graphene/h-BN/Si solar cell. Energy band structure diagram of the graphene/n-Si heterojunction without h-BN (c) and with h-BN (d) as an interlayer.

in Figure 3 (b), it is found that the cell exhibits higher EQE (30 to 50%) in the longer wavelength range of 600-800 nm. Lower EQE indicates higher recombination in the short wavelength range: 300 - 600 nm. As illustrated in Figure 3 (c), the photo-excited charge carriers are separated by the built-in electric potential (V_{bi}), where holes are pulled to the graphene electrode and the electrons towards n-Si. Here, the sum of V_{bi} and ΔE ($\Delta E = E_c - E_f$) is known as the Schottky Barrier Height (ϕ_{SBH}), which blocks the transport of electrons from n-Si back to graphene and holes from graphene back to n-Si. However, the ϕ_{SBH} is relatively low for graphene/Si heterojunction, so that electrons may drift back to graphene, and that may cause a current leakage. To reduce the current leakage, a h-BN layer is introduced between graphene and n-Si to increase the ϕ_{SBH} and thus create an extra barrier for electrons drifting back to graphene/h-BN/n-Si interface. Effective Schottky Barrier Height (ϕ'_{SBH}) in Figure 3(d) is larger than ϕ_{SBH} due to the insert of h-BN layer.

The current density-voltage (J-V) profile under dark condition is critical for understanding the electrical performance of a diode. Figure 4 (a) shows the dark J-V characteristics of the graphene/h-BN/n-Si MIS-type heterojunction cell with variation in temperature (300 K – 375 K). An increased forward current under forward bias, as well as an increased reverse current, were observed with the increased temperature for the applied voltage ranging from -0.2 V to 0.6 V. Similar phenomenon has been reported for Si-based MIS structure solar cell and graphene-based

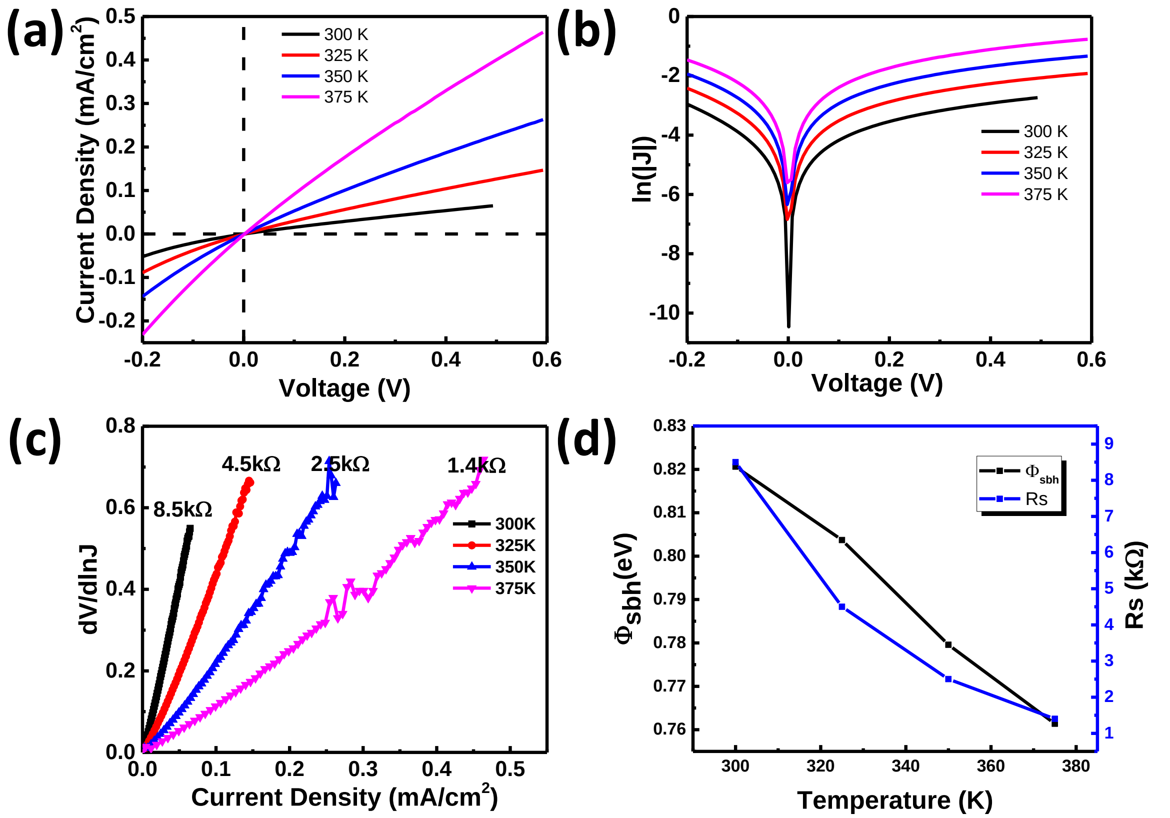

Figure 4. Temperature Dependency on Graphene/h-BN/n-Si Solar Cell without Light Illumination: (a) J-V characteristics, (b) Log(|J|)–V plot under different temperatures. (c) Series resistance derived from dark J-V characteristics. (d) The effect of temperature on Schottky Barrier Height and series resistance.

MS structure heterojunction solar cell.[42,43] As shown in Equation 6, the V_{oc} decreases as dark saturation current increases. Intrinsic carrier concentration increases as the band gap of Si decreases with the increase in temperature. The result is in accordance with realistic dark J-V characteristics.[44] Figure 4 (b) shows the log(|J|)-V plot in the voltage range of -0.2 V to 0.6 V with the increase of temperature. The series resistance was derived from the dark J-V curve as is shown in Figure 4 (c).[45] Detailed R_s values under different temperature are displayed in Figure 4 (d), the series resistance of graphene/h-BN/n-Si solar cell decreases as temperature increases. For every 25 K increase in temperature, the series resistance decreases by approximately 45%. The ϕ_{SBH} can be calculated through combining Equation (1) and (6). The ϕ_{SBH} verses temperature is plotted in Figure 4 (d), the effect of heat on ϕ'_{SBH} is plotted in Figure 3(d). The ϕ_{SBH} decreases with temperature and with the decrease of ϕ_{SBH}, electrons are easier to diffuse back to interface and recombine with holes and thus efficiency of solar cell decreased due to higher recombination.

The photovoltaic characteristics of graphene/h-BN/n-Si solar cell as a function of temperature is critical to understand the role of thermal energy in exciton carrier transport. A photovoltaic effect was obtained in Figure 5 (a) for all the temperatures studied. As shown by the gray arrow in Figure 5 (a), the V_{oc} decreases as the temperature increases. The changes of V_{oc} with temperature is plotted in Figure 5 (b) and detailed calculation is presented in the Supporting Information section 2. A linear fit was performed on data points of V_{oc} versus temperature. The R^2 is 0.999, which means the V_{oc} is linear to temperature and V_{oc} decreases by 2.0 mV for every 1 K increase in temperature. This linear property of V_{oc} versus temperature is exactly the same as the Si solar cell (2.0 mV)[42]. At the same time, J_{sc} stays almost the same (variance is 4.1×10^{-5}) when temperature increases from 300 to 375 K (Figure 5 (b)).

In order to further anaylze the effect of temperature on MIS structure graphene/h-BN/n-Si solar cell and the effect of h-BN layer, we analyzed their J-V relations as presented below:[46]

$$J = J_s exp\left(\left(\frac{V_a}{nkT}\right) - 1\right) \qquad (1)$$

$$J_s = A^*T^2 \exp\left(-\frac{q\phi_{SBH}}{kT}\right) \qquad (2)$$

Here J, J_s are the current density and reverse saturation current density respectively[17], A* is the effective Richardson constant, T is temperature, k is the Boltzmann constant, and ϕ_{SBH} is the Schottky barrier height.

The short red shift of graphene G peak indicates the lightly doped graphene, and photovoltaic effect of graphene/h-BN/n-silicon heterostructure further indicates the slightly p-doped graphene. Although graphene under ambient environment is slightly p-doped, it still behaves as a metallic electrode.[47] Adding a h-BN tunneling layer will add a tunneling probability factor $\exp\left(-\sqrt{\Delta E_c}\delta\right)$.[48] Now, the J_s can be expressed as:

$$J_s = A^*T^2 \exp\left(-\frac{q\phi_{SBH}}{kT}\right) \cdot \exp\left(-\sqrt{\Delta E_c}\delta\right) \qquad (3)$$

$$J_s = A^*T^2 \exp\left(-\frac{q\left(\phi_{SBH}+\frac{kT}{q}\sqrt{\Delta E_c}\delta\right)}{kT}\right) \qquad (4)$$

The new effective Schottky barrier height (ϕ_{SBH}') by comparing Equations (1) & (3) is:

$$\phi'_{SBH} = \phi_{SBH} + \frac{kT}{q}\sqrt{\Delta E_c}\delta \qquad (5)$$

As per the Equation 5, the effective Schottky barrier height is increased by $1.01\frac{kT}{q}\sqrt{\Delta E_c}\delta$ due to the insertion of h-BN layer. The conduction band offset (ΔE_c) represents the effective tunneling barrier height that h-BN layer creates for the electrons in the conduction band of n-Si. For graphene/h-BN/n-Si, the ΔE_c is the work function of n-Si, which is approximately 4.1 eV and δ is the thickness of the h-BN film. As is shown by the Equation 5, ΔE_c and thickness affects the J_s exponentially.

The V_{oc} of solar cell can be expressed as[49]:

$$V_{oc} = \frac{nkT}{q} \ln\left[1 + \frac{J_L}{J_s}\right] \qquad (6)$$

Here J_L is the light generated current density, J_s is the dark saturation current density, which is composed of J_{ms} (thermionic emission dark current), J_{rg} (depletion layer recombination-generation current density), J_d (injection-diffusion current density), and J_{ss} (the surface state current density due to the charge exchange between the metal and semiconductor band edges *via* surface states). We mainly focus on the effect of J_{ms} on the J_s since large J_{ms} is the main cause for the high dark current for the metal-semiconductor heterojunctions. According to Equation 4, the J_{ms} decreases with the increase of effective Schottky barrier height. Since J_L remains same for the same graphene/n-Si solar cell, the V_{oc} increases as J_s decreases with the insertion of h-BN layer in the graphene/n-Si solar cell.

The relation of saturation current density and diffusion length can be expressed as follows:[50]

$$J_s \approx \frac{qDn_i^2}{L_{diff}N} \qquad (7)$$

D is diffusivity of the minority carrier, L_{diff} is the minority carrier diffusion length, N is the doping, and n_i is the intrinsic carrier concentration. According to Equation 7, the dark saturation current density is positive dependent on n_i, and n_i increases with temperature. By combining Equation 7 and Equation for intrinsic carrier concentration, we can get Equation 8 (detail derivation is presented in the Supporting Information in which V_{oc} is linearly decreased with the temperature. The theoretic analysis is in accordance with the experiment results.

$$\frac{dV_{oc}}{dT} = -\frac{\phi'_{SBH} - V_{oc} + 3\frac{kT}{q}}{T} \qquad (8)$$

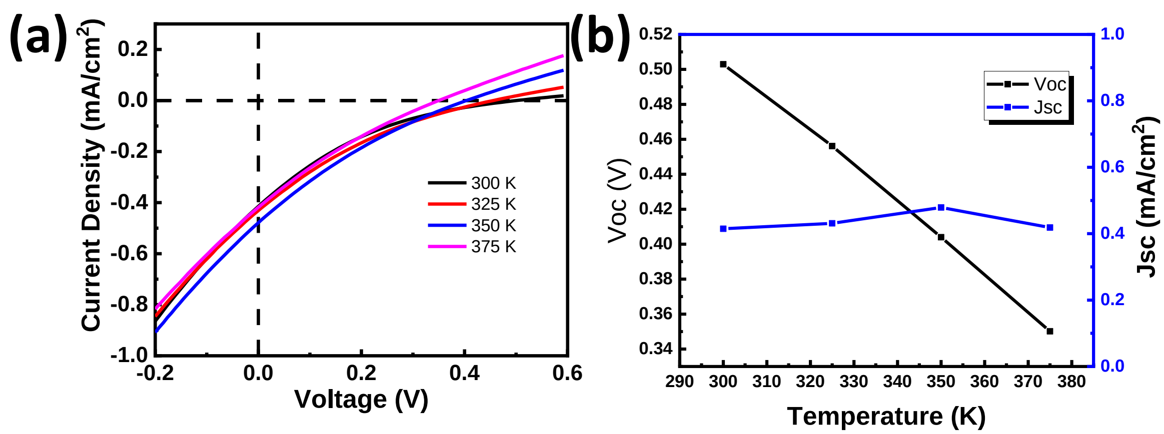

Figure 5. Temperature Dependency on Graphene/h-BN/n-Si Solar Cell under AM 1.5G Light Illumination: (a) Illuminated J-V characteristics under different temperatures. (b) V_{oc} and short circuit current density (J_{sc}) changes with temperature.

Conjointly, the interfacing of h-BN layer on n-Si passivates the surface dangling bonds. To reduce the saturation current density, longer diffusion length for the minority carriers is critically required. Diffusion length is affected by the recombination-active defects, intrinsic mobility limitation, and absence of percolation pathways. Due to the passivation of h-BN layer, dangling bonds on the Si surface will not cause the mid-gap surface states and thus recombination-active defects are reduced. Further, the MIS-type architecture is a minority carrier-based solar cell. The recombination is controlled by the number of minority carriers at the junction edge, how fast they move away from the junction and how quickly they recombine. High recombination rate increases the forward bias diffusion current, and hence increases the reverse dark-saturation current. Less reverse dark-saturation current represents a smaller number of electrons diffusing backwards and thus the chance of electrons recombining with holes gets minimized. So, smaller reverse dark saturation current means less recombination.

CONCLUSION

In summary, we have demonstrated the development of directly introduced h-BN film as a passivation and tunneling interlayer for graphene-on-Si heterojunction photovoltaic cell *via* chemical-surface-adsorption technique and investigated the temperature dependent photovoltaic characteristics of graphene/h-BN/n-Si MIS solar cell. This MIS-type heterojunction shows non-linear rectifying characteristics with increased forward current and reverse current with the increase of temperature under dark condition. Under AM 1.5G light illumination, a 4-fold increase in V_{OC} is found for the graphene/h-BN/n-Si cell compared to graphene/n-Si cell with a performance stability of 7-month. This may be due to the h-BN interlayer-induced increase in Schottky barrier height and decrease in surface mid-gap trap states. The V_{oc} was found to decrease linearly by 2.0 mV/K and J_{sc} was constant with increase in temperature. Our findings revealed the temperature dependent photovoltaic responses of the graphene/h-BN/n-Si MIS heterojunction. Further improvement can be achieved by tuning the Fermi level of graphene by doping, functionalization with nano particles and electrostatic gating. The nanoarchitecture and phenomena developed here may further provide a new avenue of designing stable, high-performance, and cost-effective tandem 2D-photovoltaic-cells.

MATERIALS AND METHODS

Direct Synthesis of h-BN on n-Si Surface. The n-Si substrates were cleaned by DI water, acetone and isopropyl alcohol (IPA). Then, they were loaded into 1 inch quartz tube inside the furnace and heated up to 1100 °C in 25 minutes with H_2 flow at 30 sccm. When the furnace temperature reached 900 °C, precursor chamber which held crucible with ammonia borane complex inside would be heated by thermal tape, whose setting temperature is 100 °C. After substrate temperature reached 1098 °C, valve connecting precursor chamber to furnace was open. Right after that, tube pressure was adjusted to 5 Torr using right angle valve near the mechanical pump. After an hour reaction, thermal tape was turned off, the valve connecting precursor chamber to furnace was closed and furnace cover was opened for fast cooling. H_2 gas was turned off when furnace temperature dropped to 60 °C and vent valve was opened to unload the sample.

Synthesis of Graphene. Pretreated copper foil was loaded in 1-inch quartz tube. The reaction chamber was evacuated to 6 mTorr and flushed with 10 sccm of H_2. Then the system was heated up to 1050 °C in 25 minutes and hold for 40 minutes with the same H_2 condition. Afterwards, the flow rate of H_2 was increased to 22 sccm and 10 sccm CH_4 was introduced for 20 seconds. Finally, the furnace was cooled down to room temperature in 35 minutes with 22 sccm H_2.

Chemical Transfer of Graphene. Copper foil with graphene was put on the spin coater (Headway Research, Inc. Model: PWM32). After its surface was covered by PMMA solution, copper foil rotated with spinner to 4000 rpm for 60 seconds. Then, copper foil was transferred to Nitric Acid Solution (30% by weight) to have copper etched away. After 10 minutes, graphene was picked by SiO_2/Si chip (3 cm*3 cm) and transferred to DI water. After cleaning in DI water for 5 minutes, graphene was transferred to second DI water and picked up by h-BN/n-Si chips from previous step. The chip was left in the hood for overnight drying. Then chip was put on hotplate which was 160 °C for 25 minutes. After that, chip was transferred to 60 °C acetone solution for 10 minutes. Finally, chip was cleaned by acetone and IPA to remove the PMMA on the top.

ASSOCIATED CONTENT

Supporting Information

Section 1: 1. Calculation of Raman spot size and pixel size. Section 2: Effect of temperature on the open-circuit voltage of graphene/h-BN/n-Si solar cell. Section 3: Derivation of V_{oc} vs. Temperature Relationship

AUTHOR INFORMATION

Corresponding Authors

*E-mail: sbehura1@uic.edu and vikasb@uic.edu

Notes

The authors declare no competing financial interests.

ACKNOWLEDGEMENTS

SKB and VB thank Dimerond Technologies, LLC for the support to conduct renewable energy research at the University of Illinois at Chicago. All the authors thank University of Illinois at Chicago for the support. VB thanks funding support from National Science Foundation (grant: 1054877) and Office of Naval Research (grants: N000141110767 and N000141812583). Authors acknowledge Michael R. Seacrist from SunEdison Semiconductor and Songwei Che for her help in device fabrications.

REFERENCES

(1) Novoselov, K. S.; Geim, A. K.; Morozov, S. V.; Jiang, D.; Zhang, Y.; Dubonos, S. V.; Grigorieva, I. V.; Firsov, A. A.; Raimond, J. M.; Brune, M.; et al. Electric Field Effect in Atomically Thin Carbon Films. *Science,* **2004**, *306* (5696), 666–669.

(2) Geim, A. K. Graphene : Status and Prospects. *Science (80-.).* **2014**, *1530* (2009), 1530–1534.

(3) Britnell, L.; Ribeiro, R. M.; Eckmann, A.; Jalil, R.; Belle, B. D.; Mishchenko, A.; Kim, Y.; Gorbachev, R. V; Georgiou, T.; Morozov, S. V; et al. Strong Light-Matter Interactions in Heterostructures of Atomically Thin Films. *Science (80-.).* **2013**, *340* (6238), 1331–1314.

(4) Li, X.; Zhu, H.; Wang, K.; Cao, A.; Wei, J.; Li, C.; Jia, Y.; Li, Z.; Li, X.; Wu, D. Graphene-on-Silicon Schottky Junction Solar Cells. *Adv. Mater.* **2010**, *22* (25), 2743–2748.

(5) Cui, T. X.; Lv, R. T.; Huang, Z. H.; Chen, S. X.; Zhang, Z. X.; Gan, X.; Jia, Y.; Li, X. M.; Wang, K. L.; Wu, D. H.; et al. Enhanced Efficiency of Graphene/Silicon Heterojunction Solar Cells by Molecular Doping. *J. Mater. Chem. A* **2013**, *1* (18), 5736–5740.

(6) Xie, C.; Lv, P.; Nie, B.; Jie, J.; Zhang, X.; Wang, Z.; Jiang, P.; Hu, Z.; Luo, L.; Zhu, Z.; et al. Monolayer Graphene Film/Silicon Nanowire Array Schottky Junction Solar Cells. *Appl. Phys. Lett.* **2011**, *99* (13).

(7) Lin, S.; Li, X.; Wang, P.; Xu, Z.; Zhang, S.; Zhong, H.; Wu, Z.; Xu, W.; Chen, H. Interface Designed MoS2/GaAs Heterostructure Solar Cell with Sandwich Stacked Hexagonal Boron Nitride. *Sci. Rep.* **2015**, *5* (May), 15103.

(8) Liu, X.; Zhang, X. W.; Meng, J. H.; Yin, Z. G.; Zhang, L. Q.; Wang, H. L.; Wu, J. L. High Efficiency Schottky Junction Solar Cells by Co-Doping of Graphene with Gold Nanoparticles and Nitric Acid. *Appl. Phys. Lett.* **2015**, *106* (23), 5.

(9) Zhang, X. X.; Xie, C.; Jie, J.; Wu, Y.; Zhang, W. High-Efficiency Graphene/Si Nanoarray Schottky Junction Solar Cells via Surface Modification and Graphene Doping. *J. Mater. Chem. A* **2013**, *1* (22), 6593.

(10) Li, X.; Xie, D.; Park, H.; Zhu, M.; Zeng, T. H.; Wang, K.; Wei, J.; Wu, D.; Kong, J.; Zhu, H. Ion Doping of Graphene for High-Efficiency Heterojunction Solar Cells. *Nanoscale* **2013**, *5* (5), 1945–1948.

(11) Che, S.; Jasuja, K.; Behura, S. K.; Nguyen, P.; Sreeprasad, T. S.; Berry, V. Retained Carrier-Mobility and Enhanced Plasmonic-Photovoltaics of Graphene via Ring-Centered H6Functionalization and Nanointerfacing. *Nano Lett.* **2017**, *17* (7), 4381–4389.

(12) Shi, E.; Li, H.; Yang, L.; Zhang, L.; Li, Z.; Li, P.; Shang, Y.; Wu, S.; Li, X.; Wei, J.; et al. Colloidal Antireflection Coating Improves Graphene-Silicon Solar Cells. *Nano Lett.* **2013**, *13* (4), 1776–1781.

(13) Lin, Y.; Li, X.; Xie, D.; Feng, T.; Chen, Y.; Song, R.; Tian, H.; Ren, T.; Zhong, M.; Wang, K.; et al. Graphene/Semiconductor Heterojunction Solar Cells with Modulated Antireflection and Graphene Work Function. *Energy Environ. Sci.* **2013**, *6* (1), 108.

(14) Yavuz, S.; Kuru, C.; Choi, D.; Kargar, A.; Jin, S.; Bandaru, P. R. Graphene Oxide as a P-Dopant and an Anti-Reflection Coating Layer, in Graphene/Silicon Solar Cells. *Nanoscale* **2016**, *8* (12), 6473–6478.

(15) He, H.; Yu, X.; Wu, Y.; Mu, X.; Zhu, H.; Yuan, S.; Yang, D. 13.7% Efficiency Graphene-Gallium Arsenide Schottky Junction Solar Cells with a P3HT Hole Transport Layer. *Nano Energy* **2015**, *16*, 91–98.

(16) Di Bartolomeo, A. Graphene Schottky Diodes: An Experimental Review of the Rectifying Graphene/Semiconductor Heterojunction. *Phys. Rep.* **2016**, *606* (May), 1–58.

(17) David, E. C:Ells: **1978**, No. 11, 1308–1317.

(18) Rupprecht, G. Cross Sections of Midgap Surface States in Silicon by Pulsed Field Effect Experiment. *J. Phys. Chem. Solids* **1960**, *14* (C), 208–213.

(19) Bullock, J.; Cuevas, A.; Yan, D.; Demaurex, B.; Hessler-Wyser, A.; De Wolf, S. Amorphous Silicon Enhanced Metal-Insulator-Semiconductor Contacts for Silicon Solar Cells. *J. Appl. Phys.* **2014**, *116* (16).

(20) Meng, J. H.; Liu, X.; Zhang, X. W.; Zhang, Y.; Wang, H. L.; Yin, Z. G.; Zhang, Y. Z.; Liu, H.; You, J. B.; Yan, H. Interface Engineering for Highly Efficient Graphene-on-Silicon Schottky Junction Solar Cells by Introducing a Hexagonal Boron Nitride Interlayer. *Nano Energy* **2016**, *28*, 44–50.

(21) Song, Y.; Li, X.; Mackin, C.; Zhang, X.; Fang, W.; Palacios, T.; Zhu, H.; Kong, J. Role of Interfacial Oxide in High-Efficiency Graphene-Silicon Schottky Barrier Solar Cells. *Nano Lett.* **2015**, *15* (3), 2104–2110.

(22) Rehman, M. A.; Akhtar, I.; Choi, W.; Akbar, K.; Farooq, A.; Hussain, S.; Shehzad, M. A.; Chun, S. H.; Jung, J.; Seo, Y. Influence of an Al2O3interlayer in a Directly Grown Graphene-Silicon Schottky Junction Solar Cell. *Carbon N. Y.* **2018**, *132*, 157–164.

(23) Zhong, M.; Xu, D.; Yu, X.; Huang, K.; Liu, X.; Qu, Y.; Xu, Y.; Yang, D. Interface Coupling in Graphene/Fluorographene Heterostructure for High-Performance Graphene/Silicon Solar Cells. *Nano Energy* **2016**, *28* (October), 12–18.

(24) Xue, J.; Sanchez-Yamagishi, J.; Bulmash, D.; Jacquod, P.; Deshpande, A.; Watanabe, K.; Taniguchi, T.; Jarillo-Herrero, P.; Leroy, B. J. Scanning Tunnelling Microscopy and Spectroscopy of Ultra-Flat Graphene on Hexagonal Boron Nitride. *Nat. Mater.* **2011**, *10* (4), 282–285.

(25) Behura, S.; Nguyen, P.; Debbarma, R.; Che, S.; Seacrist, M. R.; Berry, V. Chemical Interaction-Guided, Metal-Free Growth of Large-Area Hexagonal Boron Nitride on Silicon-Based Substrates. *ACS Nano* **2017**.

(26) Song, L.; Ci, L.; Lu, H.; Sorokin, P. B.; Jin, C.; Ni, J.; Kvashnin, A. G.; Kvashnin, D. G.; Lou, J.; Yakobson, B. I.; et al. Large Scale Growth and Characterization of Atomic Hexagonal Boron Nitride Layers. *Nano Lett.* **2010**, *10* (8), 3209–3215.

(27) Novoselov, K. S.; Jiang, D.; Schedin, F.; Booth, T. J.; Khotkevich, V. V; Morozov, S. V; Geim, A. K. (2005)Two-Dimensional Atomic Crystals.Pdf. **2005**, *102* (30), 10451–10453.

(28) Novoselov, K. S. Nobel Lecture: Graphene: Materials in the Flatland. *Rev. Mod. Phys.* **2011**, *83* (3), 837–849.

(29) Mishra, N.; Miseikis, V.; Convertino, D.; Gemmi, M.; Piazza, V.; Coletti, C. Rapid and Catalyst-Free van Der Waals Epitaxy of Graphene on Hexagonal Boron Nitride. *Carbon N. Y.* **2016**, *96*, 497–502.

(30) Meng, J. H.; Liu, X.; Zhang, X. W.; Zhang, Y. Y. Z.; Wang, H. L.; Yin, Z. G.; Zhang, Y. Y. Z.; Liu, H.; You, J. B.; Yan, H. Interface Engineering for Highly Efficient Graphene-on-Silicon Schottky Junction Solar Cells by Introducing a Hexagonal Boron Nitride Interlayer. *Nano Energy* **2016**, *28*, 44–50.

(31) Lupina, G.; Kitzmann, J.; Costina, I.; Lukosius, M.; Wenger, C.; Wolff, A.; Vaziri, S.; Östling, M.; Pasternak, I.; Krajewska, A.; et al. Residual Metallic Contamination of Transferred Chemical Vapor Deposited Graphene. *ACS Nano* **2015**, *9* (5), 4776–4785.

(32) Kalita, G.; Dzulsyahmi Shaarin, M.; Paudel, B.; Mahyavanshi, R.; Tanemura, M. Temperature Dependent Diode and Photovoltaic Characteristics of Graphene-GaN Heterojunction. *Appl. Phys. Lett.* **2017**, *111* (1).

(33) Kalita, G.; Kobayashi, M.; Shaarin, M. D.; Mahyavanshi, R. D.; Tanemura, M. Schottky Barrier Diode Characteristics of Graphene-GaN Heterojunction with Hexagonal Boron Nitride Interfacial Layer. *Phys. Status Solidi Appl. Mater. Sci.* **2018**, *215* (18), 1–6.

(34) Shewchun, J.; Singh, R.; Burk, D.; Scholz, F.; Shewchun, J.; Singh, R.; Burk, D.; Scholz, F. Temperature Dependence of the Currentvoltage Characteristics of Silicon MIS Solar Cells Temperature Dependence of the Current-Voltage Characteristics of Silicon MIS Solar Cells. **2012**, *416* (1979), 28–31.

(35) Behura, S.; Nguyen, P.; Che, S.; Debbarma, R.; Berry, V. Large-Area, Transfer-Free, Oxide-Assisted Synthesis of Hexagonal Boron Nitride Films and Their Heterostructures with MoS2 and WS2. *J. Am. Chem. Soc.* **2015**, *137* (40), 13060–13065.

(36) Reina, A.; Jia, X. T.; Ho, J.; Nezich, D.; Son, H. B.; Bulovic, V.; Dresselhaus, M. S.; Kong, J. Large Area, Few-Layer Graphene Films on Arbitrary Substrates by Chemical Vapor Deposition. *Nano Lett.* **2009**, *9* (1), 30–35.

(37) Ferrari, A. C.; Meyer, J. C.; Scardaci, V.; Casiraghi, C.; Lazzeri, M.; Mauri, F.; Piscanec, S.; Jiang, D.; Novoselov, K. S.; Roth, S.; et al. Raman Spectrum of Graphene and Graphene Layers. *Phys. Rev. Lett.* **2006**, *97* (18), 1–4.

(38) Ferrari, A. C.; Basko, D. M. Raman Spectroscopy as a Versatile Tool for Studying the Properties of Graphene. *Nat. Nanotechnol.* **2013**, *8* (4), 235–246.

(39) Reich, S.; Ferrari, A. C.; Arenal, R.; Loiseau, A.; Bello, I.; Robertson, J. Resonant Raman Scattering in Cubic and Hexagonal Boron Nitride. *Phys. Rev. B - Condens. Matter Mater. Phys.* **2005**, *71* (20), 1–12.

(40) Stenger, I.; Schué, L.; Boukhicha, M.; Berini, B.; Plaçais, B.; Loiseau, A.; Barjon, J. Low Frequency Raman Spectroscopy of Few-Atomic-Layer Thick HBN Crystals. *2D Mater.* **2017**, *4* (3), 031003.

(41) Pisana, S.; Lazzeri, M.; Casiraghi, C.; Novoselov, K. S.; Geim, A. K.; Ferrari, A. C.; Mauri, F. Breakdown of the Adiabatic Born-Oppenheimer Approximation in Graphene. *Nat. Mater.* **2007**, *6* (3), 198–201.

(42) Singh, P.; Singh, S. N.; Lal, M.; Husain, M. Temperature Dependence of I-V Characteristics and Performance Parameters of Silicon Solar Cell. *Sol. Energy Mater. Sol. Cells* **2008**, *92* (12), 1611–1616.

(43) Parui, S.; Ruiter, R.; Zomer, P. J.; Wojtaszek, M.; Van Wees, B. J.; Banerjee, T. Temperature Dependent Transport Characteristics of Graphene/n-Si Diodes. *J. Appl. Phys.* **2014**, *116* (24), 1–6.

(44) Digdaya, I. A.; Trześniewski, B. J.; Adhyaksa, G. W. P.; Garnett, E. C.; Smith, W. A. General Considerations for Improving Photovoltage in Metal-Insulator-Semiconductor Photoanodes. *J. Phys. Chem. C* **2018**, *122* (10), 5462–5471.

(45) Cheung, S. K.; Cheung, N. W. Extraction of Schottky Diode Parameters from Forward Current-Voltage Characteristics. *Appl. Phys. Lett.* **1986**, *49* (2), 85–87.

(46) Werner, J. H. Schottky Barrier and Pn-JunctionI/V Plots ? Small Signal Evaluation. *Appl. Phys. A Solids Surfaces* **1988**, *47* (3), 291–300.

(47) Piazza, A.; Giannazzo, F.; Buscarino, G.; Fisichella, G.; La Magna, A.; Roccaforte, F.; Cannas, M.; Gelardi, F. M.; Agnello, S. Effect of Air on Oxygen P-Doped Graphene on SiO2. *Phys. Status Solidi Appl. Mater. Sci.* **2016**, *213* (9), 2341–2344.

(48) Ng, K. K.; Card, H. C. Asymmetry in the SiO2 Tunneling Barriers to Electrons and Holes. *J. Appl. Phys.* **1980**, *51* (4), 2153–2157.

(49) Sinton, R. A.; Cuevas, A. Contactless Determination of Current-Voltage Characteristics and Minority-Carrier Lifetimes in Semiconductors from Quasi-Steady-State Photoconductance Data. *Appl. Phys. Lett.* **1996**, *69* (17), 2510–2512.

(50) Basore, P. A. Extended Spectral Analysis of Internal Quantum Efficiency. *Conf. Rec. Twenty Third IEEE Photovolt. Spec. Conf. - 1993 (Cat. No.93CH3283-9)* **2016**, 147–152.

(51) Brus, V. V.; Gluba, M. A.; Zhang, X.; Hinrichs, K.; Rappich, J.; Nickel, N. H. Stability of Graphene-Silicon Heterostructure Solar Cells. *Phys. Status Solidi Appl. Mater. Sci.* **2014**, *211* (4), 843–847.